



## OPEN ACCESS

EDITED BY  
Violante Di Donato,  
Unitelma Sapienza University, Italy

REVIEWED BY  
Ankit Saneja,  
Institute of Himalayan Bioresource  
Technology (CSIR), India  
Alejandro Soderini,  
University of Buenos Aires, Argentina

\*CORRESPONDENCE  
Hailin Lu  
lu@xpu.edu.cn  
Li Gao  
gaoli23@mail.xjtu.edu.cn

SPECIALTY SECTION  
This article was submitted to  
Obstetrics and Gynecological Surgery,  
a section of the journal  
Frontiers in Medicine

RECEIVED 21 October 2021  
ACCEPTED 28 June 2022  
PUBLISHED 22 July 2022

CITATION  
Zhang T, Wang L, He X, Lu H and Gao L  
(2022) Cytocompatibility  
of pH-sensitive, chitosan-coated  
Fe<sub>3</sub>O<sub>4</sub> nanoparticles in gynecological  
cells.  
*Front. Med.* 9:799145.  
doi: 10.3389/fmed.2022.799145

COPYRIGHT  
© 2022 Zhang, Wang, He, Lu and Gao.  
This is an open-access article  
distributed under the terms of the  
[Creative Commons Attribution License  
\(CC BY\)](https://creativecommons.org/licenses/by/4.0/). The use, distribution or  
reproduction in other forums is  
permitted, provided the original  
author(s) and the copyright owner(s)  
are credited and that the original  
publication in this journal is cited, in  
accordance with accepted academic  
practice. No use, distribution or  
reproduction is permitted which does  
not comply with these terms.

# Cytocompatibility of pH-sensitive, chitosan-coated Fe<sub>3</sub>O<sub>4</sub> nanoparticles in gynecological cells

Taohong Zhang<sup>1</sup>, Lisha Wang<sup>1</sup>, Xinyi He<sup>1</sup>, Hailin Lu<sup>2\*</sup> and  
Li Gao<sup>1\*</sup>

<sup>1</sup>Department of Obstetrics and Gynecology, The First Affiliated Hospital of Xi'an Jiaotong University, Xi'an Jiaotong University, Xi'an, China, <sup>2</sup>College of Mechanical and Electronic Engineering, Xi'an Polytechnic University, Xi'an, China

Nanoparticles that contact human cells without damaging basic human tissues are becoming more widely used in medicine. Efficient delivery to the intracellular target cell or compartment through the cell membrane must be achieved with minimal cytotoxicity to healthy cells. Fe<sub>3</sub>O<sub>4</sub> nanoparticles have been widely used in biomedical research for their magnetic, non-toxic, and biocompatible properties. However, the effects of Fe<sub>3</sub>O<sub>4</sub> nanoparticles coated with chitosan (CS) on gynecological cells are unclear. In this study, the Fe<sub>3</sub>O<sub>4</sub> nanoparticles were coated with CS to enhance their cytocompatibility and dispersion in water. These CS-Fe<sub>3</sub>O<sub>4</sub> nanoparticles were taken up by gynecological cells and did not affect cell viability *in vitro*. They have greater cytocompatibility in acidic environments than normal Fe<sub>3</sub>O<sub>4</sub> nanoparticles and have the potential for drug delivery into gynecological cells.

## KEYWORDS

chitosan-coated Fe<sub>3</sub>O<sub>4</sub> (CS-Fe<sub>3</sub>O<sub>4</sub>) nanoparticles, gynecological cells, cytocompatibility, ovarian cancer, gestational choriocarcinoma

## Introduction

Gynecological cancers such as cervical cancer, endometrial carcinoma, ovarian cancer, and gestational choriocarcinoma are the most common malignant diseases. They are treated by different methods, namely, surgery, radiotherapy, multichemotherapy, immunotherapy, and/or targeted therapy (1, 2). However, current treatments often negatively impact the health, fertility, and even the lifespan of women. Immunotherapy typically involves vascular endothelial growth factor, PD-1/programmed death ligand 1, tyrosine kinase, or other targeting monoclonal antibodies despite some patients not showing improvement and exhibiting serious side effects (3–7). Therefore, it is necessary to look for alternative biocompatible materials for the diagnosis, evaluation, and treatment of gynecological cancers.

In recent years, many experiments and simulation studies have focused on the influence of the physical and chemical properties of nanoparticles on cellular interactions (8–12). Superparamagnetic iron oxide materials are widely used in

drug delivery, medical imaging, cell targeting, and hyperthermia therapy (13–17). Superparamagnetic  $\text{Fe}_3\text{O}_4$  (magnetite) material is usually used in cancer hyperthermal treatment. It is of particular interest because it has far fewer side effects than chemotherapy or radiotherapy (18). Magnetite nanoparticles coated with polyarabic acid and carrying doxorubicin showed outstanding membrane permeability, excellent drug loading and release behavior, minimal *in vivo* toxicity, and promising therapeutic potential (19). The surface coating of nanoparticles also affects the interface aggregation of nanoparticles (20, 21), however, the effect on cellular uptake is unclear. The calculation model of hyperthermia has been widely used in the study of magnetite ( $\text{Fe}_3\text{O}_4$ ), maghemite ( $\text{Fe}_2\text{O}_3$ ), and various gold nanomaterial shapes (22, 23). Size-dependent nanoparticle cellular uptake through endocytosis is crucial for drug delivery in nanomedicine and a simulation of their membrane interaction may predict efficacy (24). The passive endocytosis efficiency of spherical particles is high, whereas the endocytosis of particles with sharp edges is inhibited (25).

$\text{Fe}_3\text{O}_4$  nanoparticles with a core diameter under 20 nm are usually used as tools for the diagnosis and treatment of tumors since they have unique magnetic responsiveness and photothermal effects (26–29). They are the preferred nanomaterial for MRI contrast agents since they have a strong  $T_2$  relaxation signal (30) and are safe for use in humans due to the efficient biodegradation of the free ions (31–33).  $\text{Fe}_3\text{O}_4$  nanoparticles require appropriate surface functionalization to prevent them from being cleared from the circulatory system by the immune system (34). Chitosan (CS) is the second-largest natural cationic polysaccharide and is renewable, biodegradable, non-toxic, and has biocompatible properties (35–38). CS has abundant functional groups on its surface; thus, CS- $\text{Fe}_3\text{O}_4$  nanoparticles can interact with other molecules and potentially deposit a variety of inorganic and organic materials *in vivo*. In this study, the sol-gel method was successfully used to prepare CS- $\text{Fe}_3\text{O}_4$  nanoparticles. As a result, the  $\text{Fe}_3\text{O}_4$  nanoparticles were wrapped by CS. Their biocompatibility is greater than that of inorganic nanoparticles, which reflects their appreciable clinical application potential (39, 40). In addition, CS has abundant functional groups on its surfaces, meaning that the CS- $\text{Fe}_3\text{O}_4$  nanoparticles are able to interact with other molecules and can easily deposit a variety of inorganic and organic materials.

In this study, CS- $\text{Fe}_3\text{O}_4$  nanoparticles were analyzed using scanning electron microscopy (SEM), transmission electron microscopy (TEM), Fourier transform infrared (FT-IR) spectroscopy, X-ray photoelectron spectroscopy (XPS), thermogravimetric analysis (TG), and differential scanning calorimetry (DSC). Then, the methyl thiazolyl tetrazolium (MTT) method was used to test the toxicity of gynecological cells, and cell viability data were measured.

Due to their low toxicity properties, these CS- $\text{Fe}_3\text{O}_4$  nanoparticles may have excellent performance in the encapsulation and release of drugs, in nanoparticle targeting, medical imaging, cell targeting, and hyperthermia therapy.

## Materials and methods

### Materials

$\text{FeCl}_3 \cdot 6\text{H}_2\text{O}$  and ammonia solution (25%) were purchased from Damao Chemical Reagent Factory, Tianjin, China.  $\text{FeCl}_2 \cdot 4\text{H}_2\text{O}$  was from Tianjin Guangfu Fine Research Institute, Tianjin, China. Acetic acid was from Fuyu Fine Chemical Co., Ltd., Tianjin, China. CS (degree of deacetylation  $\geq 90\%$ ; molecular weight, 700–800 kDa) was purchased from Shanghai Lanji Technology Co., Ltd. (Shanghai, China). All materials used in the research were of analytical reagent grade.

### Cell culture

The SKOV-3 adherent human ovarian cancer cell line and the JEG-3 human choriocarcinoma cell line were obtained from the Shanghai Cell Bank of the Chinese Academy of Sciences (Shanghai, China). The CAO-3 human ovarian cancer cell line was purchased from Procell Life Science & Technology Co., Ltd. The A2780 human ovarian cancer cell line was obtained from the Shandong Academy of Medical Sciences (Jinan, China). The human first-trimester extravillous trophoblast cell line (HTR-8) was obtained from the American Type Culture Collection (Manassas, VA, United States), and the JAR human choriocarcinoma cell line was obtained from the Beijing Cell Bank of the Chinese Academy of Sciences (Beijing, China). HTR-8, JAR, and A2780 cells were cultured in RPMI-1640 medium with 10% fetal bovine serum and an antibiotic solution (100 U/ml penicillin and 100  $\mu\text{g}/\text{ml}$  streptomycin) at 37°C in a 5%  $\text{CO}_2$  atmosphere, and JEG-3, SKOV-3, and CAO-3 cells were cultured in Dulbecco's Modified Eagle Medium (DMEM; Gibco, Grand Island, NY, United States) with 10% fetal bovine serum and an antibiotic solution (100 U/ml penicillin and 100  $\mu\text{g}/\text{ml}$  streptomycin) at 37°C in a 5%  $\text{CO}_2$  atmosphere. The cell experiments were carried out in the Department of Obstetrics and Gynecology, The First Affiliated Hospital of Xi'an Jiaotong University, China.

RPMI-1640 medium or DMEM medium with 10% fetal bovine serum was prepared at different pH values by the addition of acetic acid or sodium bicarbonate to obtain pH values of 5.5, 6, 6.5, 7, or 7.5 followed by filtering with 0.22- $\mu\text{m}$  diameter filters (Millipore, MA, United States) into sterile glass bottles.

## Preparation of CS-Fe<sub>3</sub>O<sub>4</sub> nanoparticles

In total, 1 g of ferric chloride hexahydrate and 0.5 g of ferrous chloride tetrachloride were dissolved in 50 ml of deionized water. Then, 50 ml of 1% w/v CS sol was prepared by dissolving CS in 1% w/v acetic acid. The iron ion solution was added to the CS sol, and the temperature was increased to 75°C under a magnetic field. Ammonia solution was added with stirring until the solution turned black and stirring was continued for 0.5 h. The precipitate was centrifuged at 3,750 g for 30 min and then repeatedly washed with deionized water until a neutral pH was obtained. Finally, CS-Fe<sub>3</sub>O<sub>4</sub> nanoparticles were lyophilized. Fe<sub>3</sub>O<sub>4</sub> nanoparticles were prepared using the above method described without CS addition.

## Characterization of CS-Fe<sub>3</sub>O<sub>4</sub> nanoparticles

Fourier transform infrared spectroscopy (FT-IR) was performed using a Nicolet iS50 spectrometer (Thermo Fisher Scientific, MA, United States). XPS was performed with an ESCALAB 250 Xi<sup>+</sup> XPS instrument (Thermo Fisher Scientific, MA, United States). X-ray diffraction (XRD) was performed with a D8 Advance system (Bruker, Germany). TG and DSC analyses were performed under an oxygen atmosphere using a simultaneous thermal analyzer 409 CD (Netzsch-Gerätebau GmbH, Germany). CS-Fe<sub>3</sub>O<sub>4</sub> nanoparticles were thoroughly dissolved in 1% w/v acetic acid and observed with an H-7650 transmission electron microscope (Hitachi, Tokyo, Japan). The morphology of Fe<sub>3</sub>O<sub>4</sub> and CS-Fe<sub>3</sub>O<sub>4</sub> nanoparticles was determined by SEM with a SU3500 instrument (Techcomp, Shanghai, China).

## Cytocompatible tests

### Methyl thiazolyl tetrazolium assay

A modified MTT [3-(4,5-dimethylthiazole-2-yl)-2,5-diphenyltetrazolium bromide] assay was performed to measure cell viability according to the manufacturer's instructions. In brief, HTR-8, JAR, A2780, and SKOV-3 cells were seeded at a density of  $4 \times 10^3$  cells per well in 96-well plates, while JEG-3 and CAOV-3 cells were seeded at a density of  $6 \times 10^3$  cells per well, then treated with different concentrations of Fe<sub>3</sub>O<sub>4</sub> and CS-Fe<sub>3</sub>O<sub>4</sub> (0–10 µg/ml) for 24 and 48 h, respectively. In addition, SKOV-3 and CAOV-3 cells were incubated with Fe<sub>3</sub>O<sub>4</sub> and CS-Fe<sub>3</sub>O<sub>4</sub> (10 µg/ml) at different pH values for the same duration. Then, 20 µl MTT (5 mg/ml) was added to 180 µl complete medium per well and incubated for 4 h. The medium was removed, then 130 µl of DMSO

was added to each well, the plates were shaken for 10 min, and the absorbance at 490 nm was measured using an xMark microplate absorbance spectrophotometer (Bio-Rad, Hercules, CA, United States). The experiments were conducted in triplicate and the values are expressed as the mean  $\pm$  standard error.

### Flow cytometry analysis

SKOV-3 cells ( $5 \times 10^4$ ) were placed in 500 µl of complete media seeded into 6-well plates and treated with Fe<sub>3</sub>O<sub>4</sub> and CS-Fe<sub>3</sub>O<sub>4</sub> (10 µg/ml) at different pH values for 48 h before performing cell cycle arrest analysis. The cells were harvested *via* centrifugation at 1,000 rpm for 5 min at room temperature, washed with ice-cold phosphate-buffered saline (PBS; 137 mM NaCl, 2.7 mM KCl, 10 mM Na<sub>2</sub>HPO<sub>4</sub>, and 2 mM KH<sub>2</sub>PO<sub>4</sub> pH 7.2) three times, then fixed with 70% ethanol at 4°C overnight. Fixed cells were treated with 100 µg/ml propidium iodide (PI) and 100 µg/ml RNase A in PBS and incubated at room temperature for 25 min. Finally, cell cycle arrest was analyzed using a FACSCalibur cell sorter (BD Biosciences, Franklin Lakes, NJ, United States) and CellQuest software version 3.3 (BD Biosciences) according to the manufacturer's instructions.

### Calcein-AM/PI staining for viable and dead cells

SKOV-3 cells ( $2 \times 10^4$ ) were placed in 500 µl of complete media, seeded into 24-well plates, and treated with Fe<sub>3</sub>O<sub>4</sub> and CS-Fe<sub>3</sub>O<sub>4</sub> (10 µg/ml) at different pH values for 24 h. The culture medium was removed, gently washed two to three times with PBS, and stained with assay solution (2 µl/ml calcein-AM and 1 µl/ml PI) according to the manufacturer's instructions (MoBiTec GmbH, Göttingen, Germany) at 37°C for 15 min. The digital images of viable cells (green fluorescence, excitation wavelength: 490 nm, emission wavelength: 515 nm) and dead cells (red fluorescence, excitation wavelength: 535 nm, emission wavelength: 617 nm) were visualized using a fluorescence microscope. This experiment was performed in triplicate.

The cell experiments were carried out at the First Affiliated Hospital of Xi'an Jiaotong University, China.

## Results and discussion

### Scanning electron microscopy and transmission electron microscopy analyses

The synthesized Fe<sub>3</sub>O<sub>4</sub> nanoparticles show an apparent resemblance to small balls of aggregates (Figure 1a) which is verified by the high-resolution SEM image (Figure 1b). The CS-Fe<sub>3</sub>O<sub>4</sub> nanoparticles have an evident polymer (Figure 1c) coating with an approximate size of 10 nm (Figure 1d).

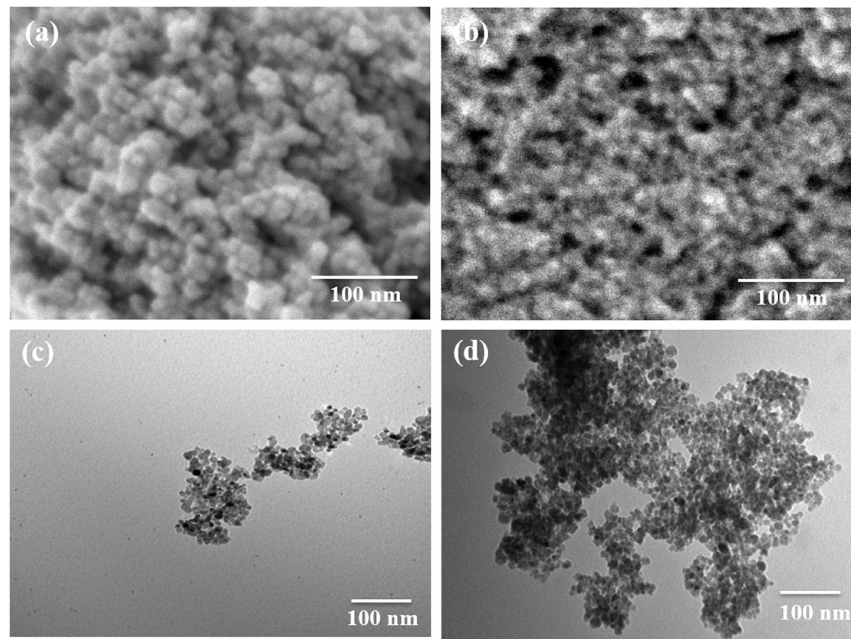


FIGURE 1

Morphology of  $\text{Fe}_3\text{O}_4$  and  $\text{CS-Fe}_3\text{O}_4$  nanoparticles. (a) High-resolution scanning electron microscopy (SEM) image of  $\text{Fe}_3\text{O}_4$  nanoparticles. (b) High-resolution SEM image of  $\text{CS-Fe}_3\text{O}_4$  nanoparticles. (c) Transmission electron microscopy (TEM) image of  $\text{Fe}_3\text{O}_4$  nanoparticles. (d) TEM image of  $\text{CS-Fe}_3\text{O}_4$  nanoparticles.

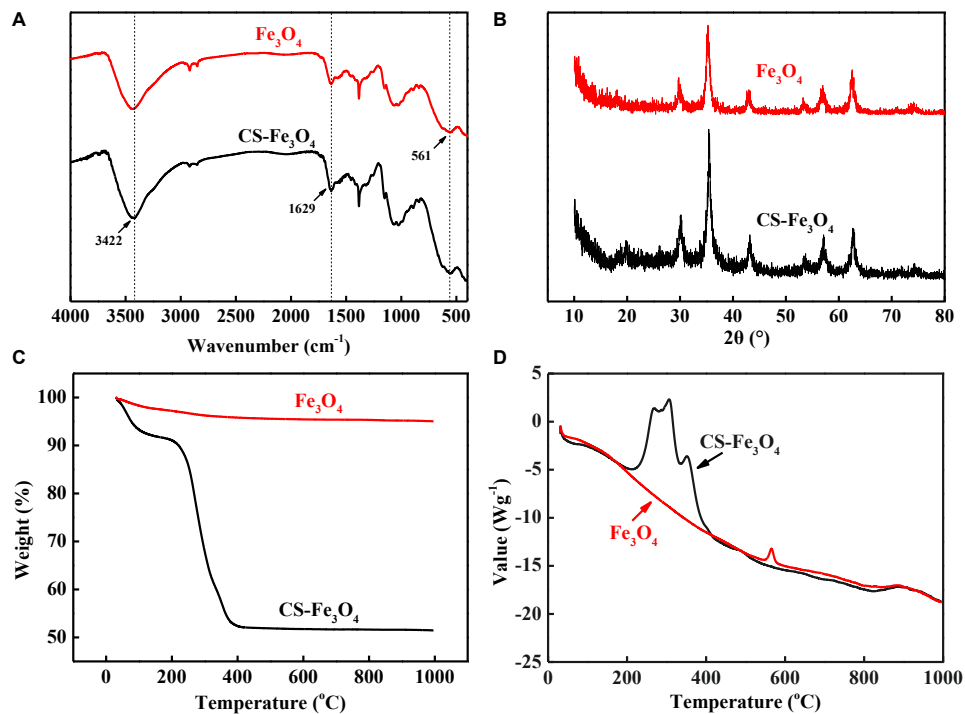


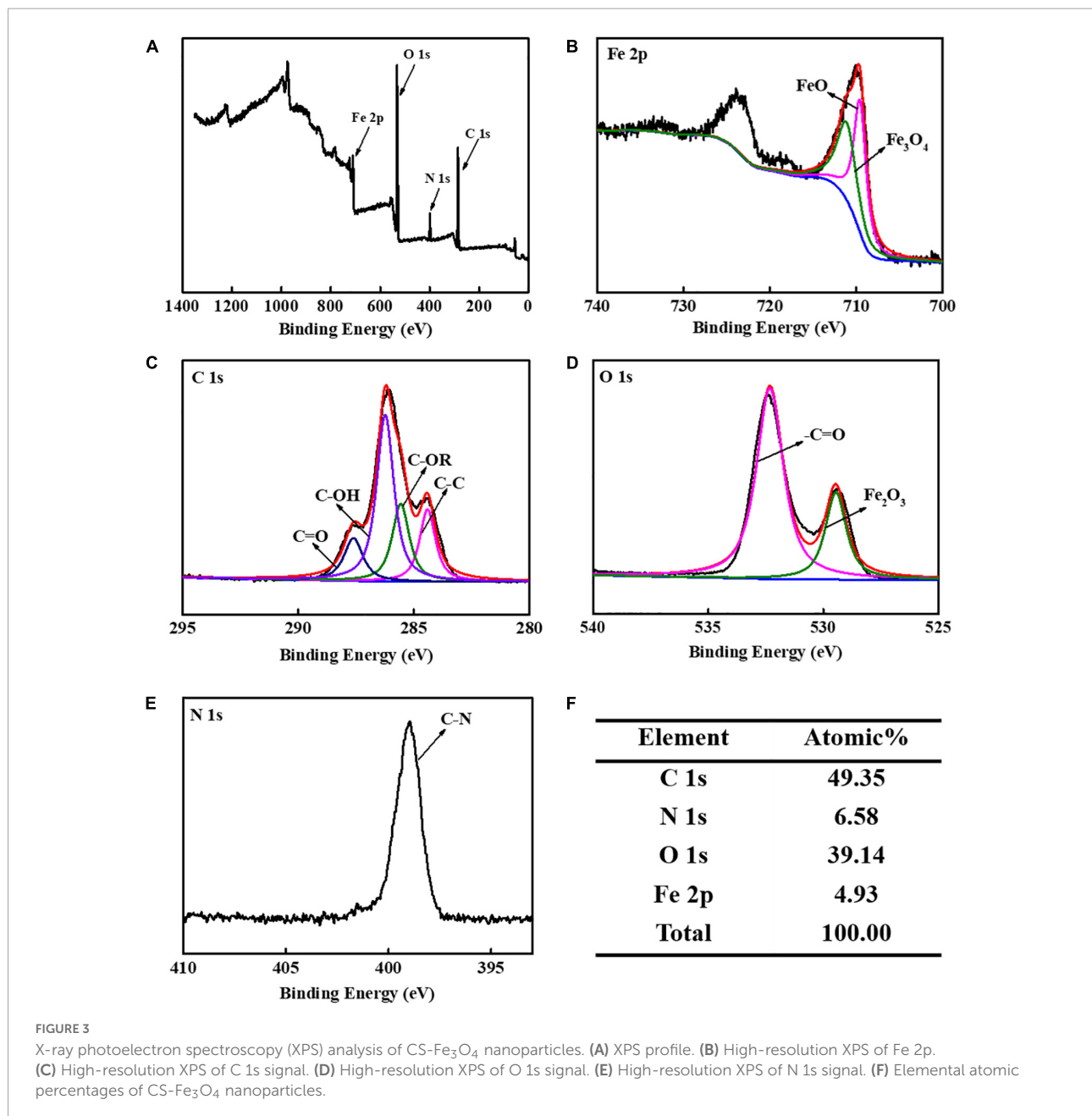
FIGURE 2

(A) Fourier transform infrared (FT-IR) spectra. (B) High-resolution X-ray diffraction (XRD) spectra of C 1s signals. (C) Thermogravimetric analysis (TG) curves. (D) Differential scanning calorimetry (DSC) curves of  $\text{CS-Fe}_3\text{O}_4$  nanoparticles.

**Figure 1** shows the morphology of the  $\text{Fe}_3\text{O}_4$  and CS- $\text{Fe}_3\text{O}_4$  nanoparticles. The SEM image in **Figure 1a** depicts the morphology of the synthesized  $\text{Fe}_3\text{O}_4$  nanoparticles which shows an apparent resemblance to small balls aggregation. This is further confirmed by the high-resolution SEM imaging shown in **Figure 1b**, which also shows the state of aggregation by small balls. In **Figure 1c**, the SEM image of the CS- $\text{Fe}_3\text{O}_4$  nanoparticles can be seen with evident polymer covering. In **Figure 1d**, the CS- $\text{Fe}_3\text{O}_4$  nanoparticles exhibit evidence the covering of CS and the nanoparticles are  $\sim 10$  nm, and therefore, it can be inferred that the CS can effectively isolate the  $\text{Fe}_3\text{O}_4$  nanoparticles.

## Fourier transform infrared spectroscopy, X-ray photoelectron spectroscopy, thermogravimetric analysis, and differential scanning calorimetry analyses

The infrared spectrum peaks at  $3,422$  and  $1,629$   $\text{cm}^{-1}$  in  $\text{Fe}_3\text{O}_4$  and CS- $\text{Fe}_3\text{O}_4$  nanoparticles are attributed to the O-H stretching vibration of water and the H-O-H bending vibration of water, respectively (**Figure 2A**) (41). The peak at  $561$   $\text{cm}^{-1}$  is attributed to  $\text{Fe}_3\text{O}_4$  (41). The diffraction peaks observed in the CS- $\text{Fe}_3\text{O}_4$  composite in **Figure 2B**



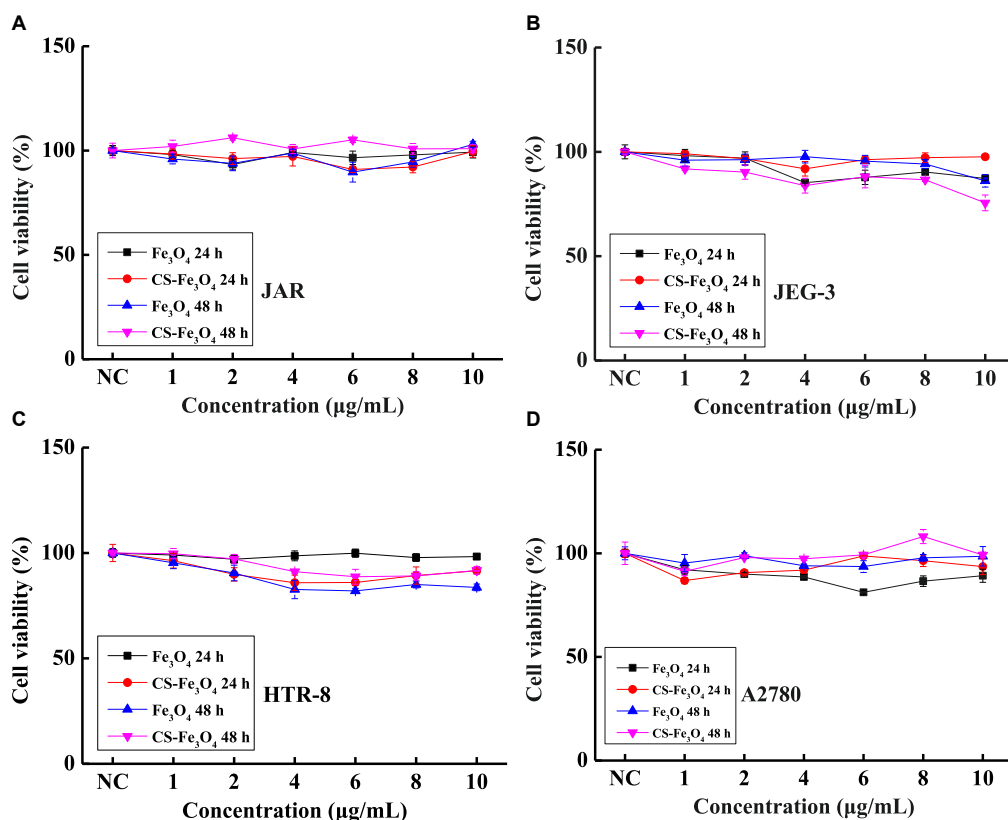


FIGURE 4 Cell viability of (A) JAR cells, (B) JEG-3 cells, (C) HTR-8 cells, and (D) A2780 cells with Fe<sub>3</sub>O<sub>4</sub> and CS-Fe<sub>3</sub>O<sub>4</sub> nanoparticles under different concentrations and treatment periods.

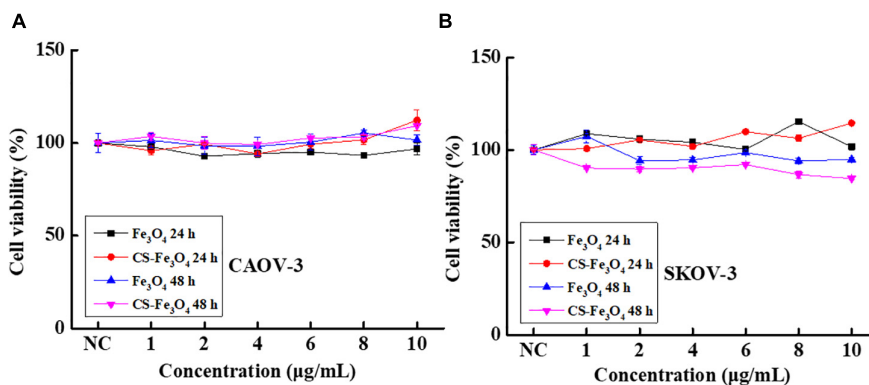


FIGURE 5 Cell viability of (A) CAOV-3 cells and (B) SKOV-3 cells with Fe<sub>3</sub>O<sub>4</sub> and CS-Fe<sub>3</sub>O<sub>4</sub> nanoparticles under different concentrations and treatment periods.

(2θ = 30.1°, 35.5°, 42.9°, 53.3°, 57.1°, and 62.7°) were assigned to the following diffraction planes of the cubic spinel crystal structure of Fe<sub>3</sub>O<sub>4</sub>, respectively: (220), (311), (400), (422), (511), and (440) (JCPDS file no. 19-0629). The above data demonstrate that Fe<sub>3</sub>O<sub>4</sub> in the CS-Fe<sub>3</sub>O<sub>4</sub> composite had the

same physical and chemical properties as standard Fe<sub>3</sub>O<sub>4</sub>. CS-Fe<sub>3</sub>O<sub>4</sub> nanoparticles contained approximately 43.5% of CS and had a sharp weight loss between 215 and 397°C by TGA (Figure 2C), which is attributed to CS decomposition. The TG curve became stable at 420°C with 51.5% solid residue

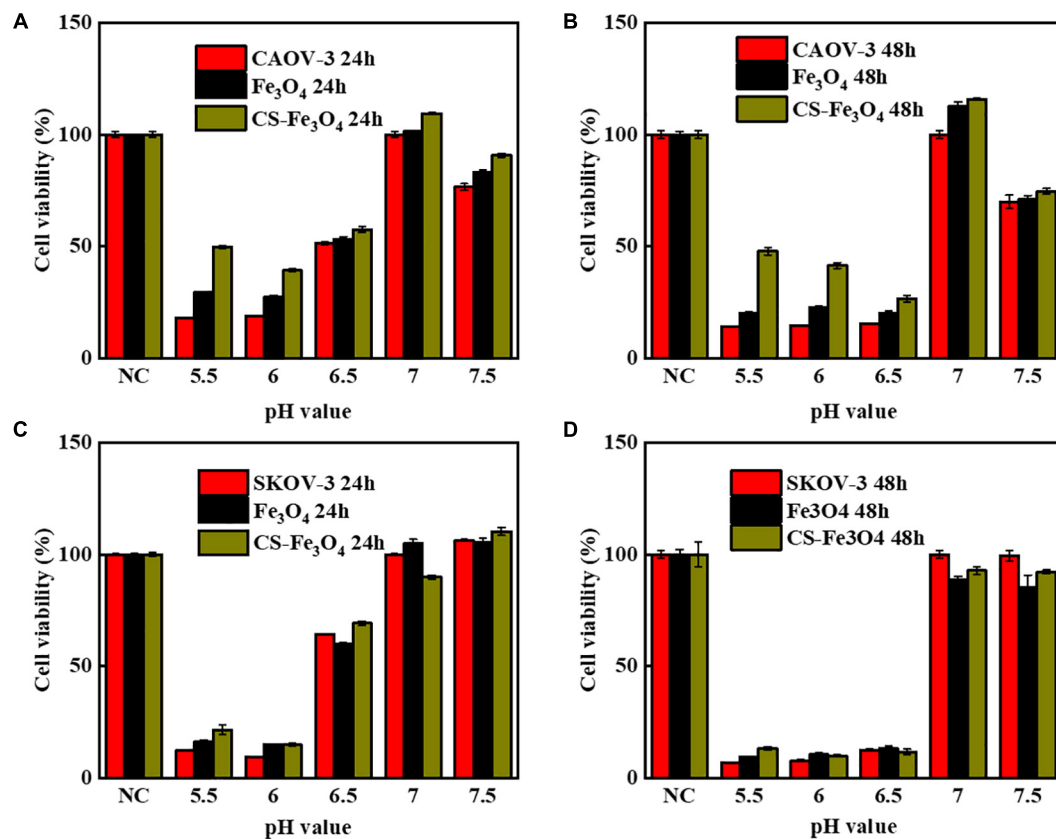


FIGURE 6

Cell viability of (A) CAOV-3 cells treated for 24 h, Fe<sub>3</sub>O<sub>4</sub> treated for 24 h, and CS-Fe<sub>3</sub>O<sub>4</sub> treated for 24 h; (B) CAOV-3 cells treated for 48 h, Fe<sub>3</sub>O<sub>4</sub> treated for 48 h, and CS-Fe<sub>3</sub>O<sub>4</sub> treated for 48 h; (C) SKOV-3 cells treated for 24 h, Fe<sub>3</sub>O<sub>4</sub> treated for 24 h, and CS-Fe<sub>3</sub>O<sub>4</sub> treated for 24 h; (D) SKOV-3 cells treated for 48 h, Fe<sub>3</sub>O<sub>4</sub> treated for 48 h, and CS-Fe<sub>3</sub>O<sub>4</sub> treated for 48 h at different pH values.

remaining at 1,000°C. Meanwhile, Fe<sub>3</sub>O<sub>4</sub> nanoparticles showed a slight weight decrease between 30 and 1,000°C with 95% solid residue remaining at 1,000°C. The exothermic range of CS-Fe<sub>3</sub>O<sub>4</sub> nanoparticles observed at 215–411°C by DSC (Figure 2D) confirmed that they started to react with the air and decomposed from approximately 215°C, followed by a sharper and stronger decomposition at ~308°C. Meanwhile, Fe<sub>3</sub>O<sub>4</sub> nanoparticles had a stable endothermic DSC curve except for a small exothermic peak at 564°C. In conclusion, the TG and DSC results proved that the CS-Fe<sub>3</sub>O<sub>4</sub> nanoparticles contained abundant CS.

## X-ray photoelectron spectroscopy analysis

The CS-Fe<sub>3</sub>O<sub>4</sub> nanoparticles have evident C 1s, N 1s, O 1s, and Fe 2p signals (Figure 3A). The high-resolution XPS of Fe 2p was found in two groups: Fe<sub>3</sub>O<sub>4</sub> 711.3 eV and FeO 709.6 eV (Figure 3B). The fitted C 1s peaks of C=O, C–OH, C–OR, and C–C are observed at 287.6, 286.2, 285.6, and 284.4 eV,

respectively, which is within 0.2 of the standard peaks: 287.8, 286.4, 285.4, and 284.6 eV, respectively (Figure 3C). The O 1s fitted peaks at 532.3 and 529.5 eV are attributed to –C=O and Fe<sub>2</sub>O<sub>3</sub>, respectively (Figure 3D), confirming that synthesized CS-Fe<sub>3</sub>O<sub>4</sub> nanoparticles contain CS and Fe<sub>2</sub>O<sub>3</sub>. The peak at 398.9 eV attributed to C–N (Figure 3E) supported the presence of CS in CS-Fe<sub>3</sub>O<sub>4</sub> nanoparticles. The C 1s signal occupies 49.35% of the atomic composition showing that CS efficiently covers the Fe<sub>3</sub>O<sub>4</sub> nanoparticles (Figure 3F).

## Cell viability

The cell viabilities of JAR (Figure 4A), JEG-3 (Figure 4B), HTR-8 (Figure 4C), and A2780 (Figure 4D) cells were measured after being incubated with various concentrations of the CS-Fe<sub>3</sub>O<sub>4</sub> nanoparticles for 24 and 48 h. Figure 4 shows that the CS-Fe<sub>3</sub>O<sub>4</sub> nanoparticles have good biocompatibility for gynecological cells. The cell viabilities of cancer cells (JAR, JEG-3, HTR-8, and A2780 cells) were estimated to be more than 80% when the concentrations were increased to 10 μg/ml,

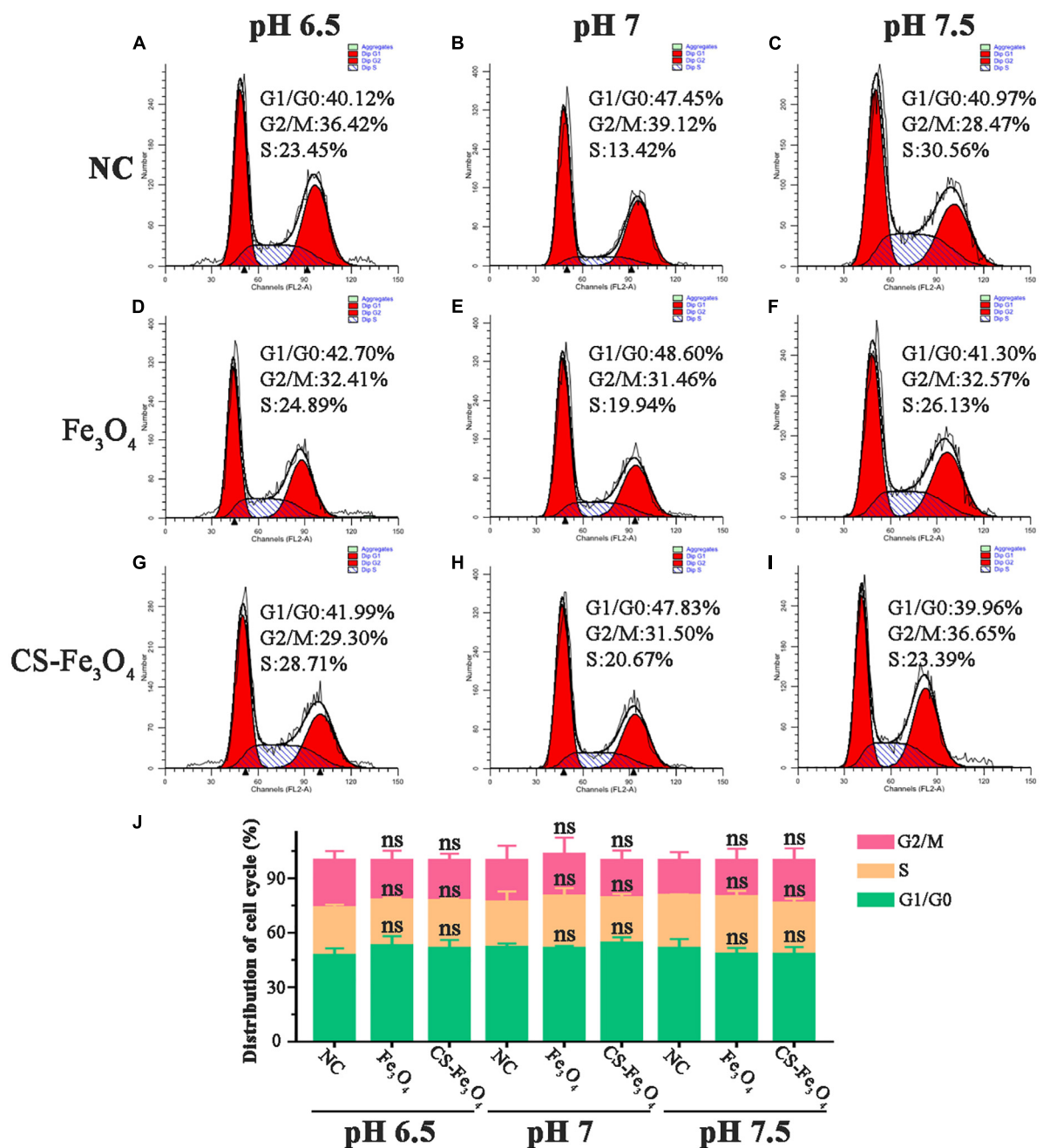


**FIGURE 7** Cell flow cytometry analysis of SKOV-3 cells (A–C) NC, (D–F) Fe<sub>3</sub>O<sub>4</sub> nanoparticles, and (G–I) CS-Fe<sub>3</sub>O<sub>4</sub> nanoparticles at different pH values 24 h after treatment. (J) The cell cycle distributions were analyzed in the histogram. ns: no statistical difference.

and the normal cell viabilities of HTR-8 (Figure 4C) were estimated to be more than 83% when the concentrations were increased to 10 μg/ml. For the same condition, no obvious cell viability change was observed in CAOV-3 cells (Figure 5A). There was a slight decrease in the viability of SKOV-3 cells at 48 h (Figure 5B). These results indicate distinctive cell growth, and a minimal toxicity effect can be achieved with

the nanoparticles. The above data revealed that the Fe<sub>3</sub>O<sub>4</sub> and CS-Fe<sub>3</sub>O<sub>4</sub> nanoparticles all have good cytocompatibility.

All the above-mentioned results indicate that, in normal conditions, Fe<sub>3</sub>O<sub>4</sub> and CS-Fe<sub>3</sub>O<sub>4</sub> nanoparticles have good cytocompatibility. The cytotoxicity test results showed that the Fe<sub>3</sub>O<sub>4</sub> and CS-Fe<sub>3</sub>O<sub>4</sub> nanoparticles had a strong increasing effect on cell viability under different pH value conditions, and

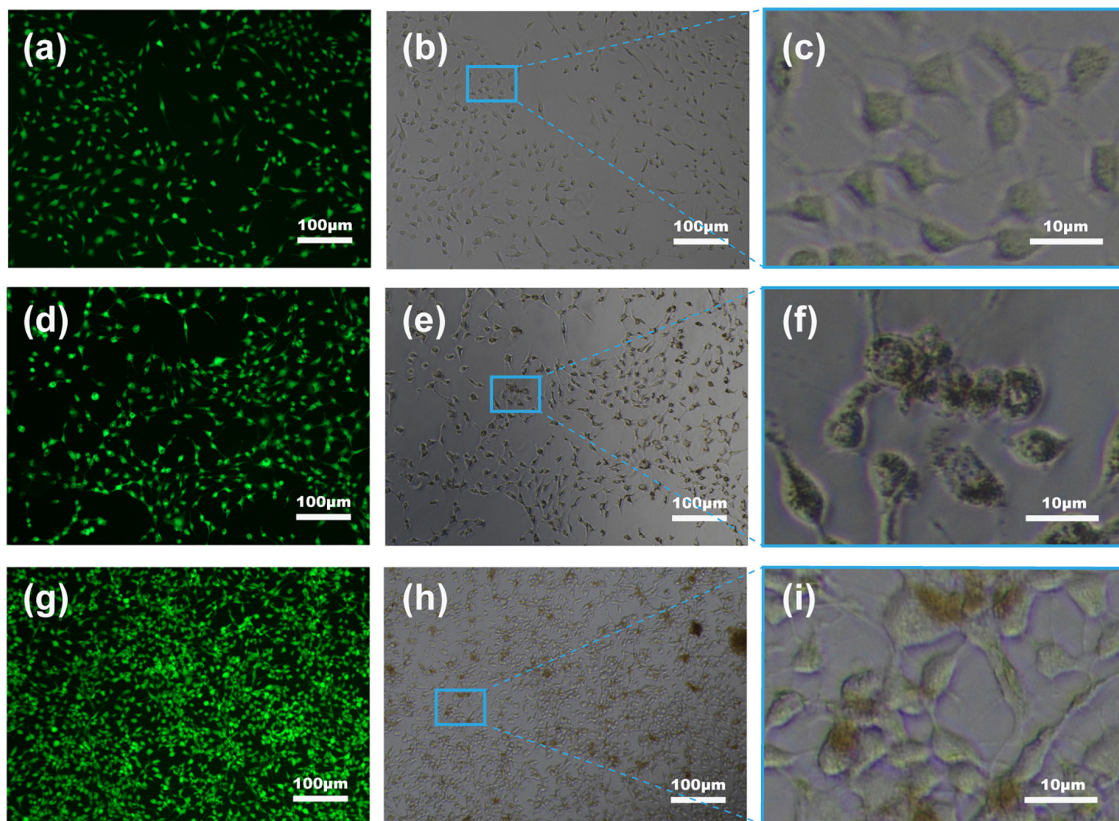


FIGURE 8

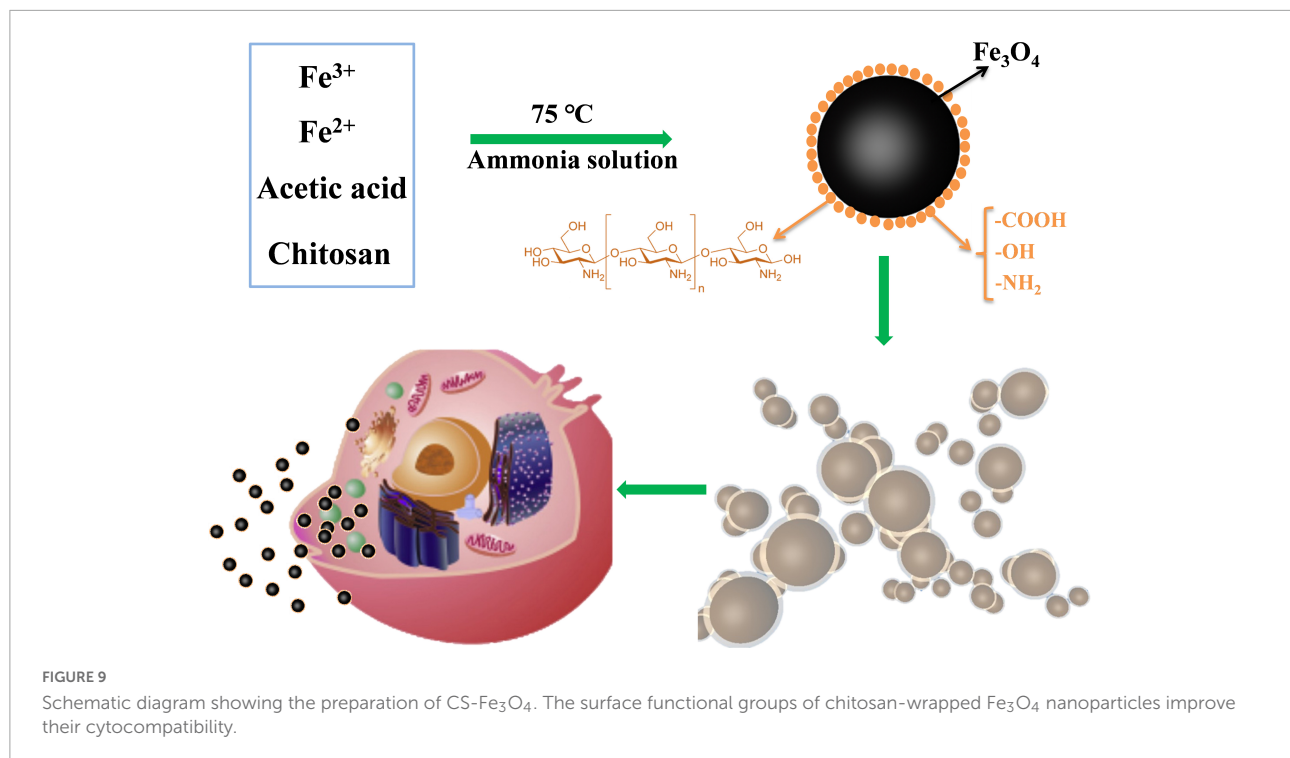
Fluorescent images of SKOV-3 cells following staining with calcein AM. (a–c) NC, (d–f)  $\text{Fe}_3\text{O}_4$  nanoparticles, and (g–i) CS- $\text{Fe}_3\text{O}_4$  nanoparticles at pH 7 after 24 h after treatment.

that the cell survival rate decreased significantly as the pH value decreased (Figure 6). The CAOV-3 and SKOV-3 cells had high cell viability at pH values 6.5, 7, and 7.5 after 24 h, but the cell viability at pH value 6.5 was obviously decreased at 48 h. The survival rate of the CAOV-3 (Figure 6A) and SKOV-3 (Figure 6C) cells were below 20% at pH 5.5 and pH 6 after 24 h, and the cell viability was further decreased at 48 h (Figures 6B,D). The above results revealed that an acid environment considerably impacts cell viability, and that CS- $\text{Fe}_3\text{O}_4$  nanoparticles can efficiently improve cell viability in an acidic environment.

The results of the MTT test revealed that the cell viability of SKOV-3 cells varied in  $\text{Fe}_3\text{O}_4$  and CS- $\text{Fe}_3\text{O}_4$  treatments under acidic environments. Therefore, we hypothesized that  $\text{Fe}_3\text{O}_4$  and CS- $\text{Fe}_3\text{O}_4$  may influence gynecology cell proliferation under a lower pH level. Therefore, the cell cycle was detected using flow cytometry to observe the cell viability of SKOV-3 cells at different pH values after 24 h. As shown in Figures 7A–C, the cell cycle of SKOV-3 cells was identified in the NC group. The percentage of cell cycle SKOV-3 cells following the addition of  $\text{Fe}_3\text{O}_4$  (Figures 7D–F) and CS- $\text{Fe}_3\text{O}_4$  (Figures 7G–I) nanoparticles was stable (10  $\mu\text{g}/\text{ml}$ ) at different

pH values. Compared to the NC group under pH 6.5 and pH 7, neither  $\text{Fe}_3\text{O}_4$  nor CS- $\text{Fe}_3\text{O}_4$  caused phase arrest in SKOV-3 cells after 24 h of exposure (Figure 7J). In addition, there were no apoptotic changes, such as cell shrinkage, in SKOV-3 cells treated for 24 h with  $\text{Fe}_3\text{O}_4$  or CS- $\text{Fe}_3\text{O}_4$  (10  $\mu\text{g}/\text{ml}$ ), as identified using EDU staining (Supplementary Figure 4). Of course, there were no statistical differences in the cell cycle at different pH values. This indicates that  $\text{Fe}_3\text{O}_4$  and CS- $\text{Fe}_3\text{O}_4$  do not play a role in cell cycles at low pH levels.

Untreated living cells have weak fluorescence following staining with calcein AM with only some of the non-fluorescent intracellular dye converted to a green, fluorescent substance (Ex/Em: 495/520 nm) by intracellular esterases due to partial permeability of the membrane (Figure 8a). The greater signal in  $\text{Fe}_3\text{O}_4$  treatment (Figure 8d) and especially CS- $\text{Fe}_3\text{O}_4$  treatment (Figure 8g) indicates nanoparticles have facilitated a greater uptake of this dye cells compared with the NC (Figure 8c). Moreover, compared with the NC (Figure 8b), SKOV-3 cells efficiently uptake  $\text{Fe}_3\text{O}_4$  and CS- $\text{Fe}_3\text{O}_4$  nanoparticles (Figures 8e,h), as shown better in the high magnification (Figures 8f,i). The addition of PI detects damaged cell membranes (or dead cells) by binding to nucleic acids and



producing a bright red fluorescent signal (Ex/Em: 530/620 nm) (Supplementary Figures 1–3). The small fluorescent red dots shown in Supplementary Figures 2, 3 indicate that SKOV-3 cell death did not occur. This phagocytosis effect means that the drugs can easily enter cells when they are combined with these nanoparticles. The above data indicate that the cells had high survival rates after phagocytizing abundant quantities of Fe<sub>3</sub>O<sub>4</sub> and CS-Fe<sub>3</sub>O<sub>4</sub> nanoparticles.

## Relevant mechanisms

Chitosan (CS) has strong intramolecular and intermolecular hydrogen bonding interactions in its structure; therefore, it cannot be dissolved in water (35, 38). In this work, one % w/v acetic acid was used to dissolve CS, followed by the addition of Fe<sup>3+</sup> and Fe<sup>2+</sup> (Figure 9). Fe<sub>3</sub>O<sub>4</sub> was formed when the ammonia solution was added at 75°C, and CS was simultaneously recrystallized because of the acid loss. The CS-Fe<sub>3</sub>O<sub>4</sub> nanoparticles prepared using this method are smaller than those produced *via* the conventional co-precipitation method and are expected to improve the deposition of medicinal drugs. Engulfment of Fe<sub>3</sub>O<sub>4</sub> molecules by CS prevents agglomeration between nanoparticles, and the biocompatible CS surface is beneficial to cytophagocytosis (Figure 9). The CS-Fe<sub>3</sub>O<sub>4</sub> nanoparticles have better biodegradability and biocompatibility than Fe<sub>3</sub>O<sub>4</sub> because the organic surface has abundant functional groups that can deposit various materials.

## Conclusion

In this experiment, the sol-gel method was successfully used to prepare Fe<sub>3</sub>O<sub>4</sub> nanoparticles, and CS was used to engulf Fe<sub>3</sub>O<sub>4</sub> nanoparticles. The CS-Fe<sub>3</sub>O<sub>4</sub> nanoparticles were characterized by SEM, TEM, FT-IR, XPS, TG, and DSC and compared with Fe<sub>3</sub>O<sub>4</sub>. The CS-Fe<sub>3</sub>O<sub>4</sub> nanoparticles are biocompatible with gynecological cells *in vitro* and exhibit higher viability than Fe<sub>3</sub>O<sub>4</sub> nanoparticles at different pH values. CS-Fe<sub>3</sub>O<sub>4</sub> nanoparticles phagocytized by gynecological cells do not affect cell viability. These properties favor CS-Fe<sub>3</sub>O<sub>4</sub> nanoparticles for the deposition of various materials such as drugs in cellular compartments. Further *in vivo* studies are required to determine the applicability of this nanoparticle for cell targeting, hyperthermia therapy, and medical imaging.

## Data availability statement

The original contributions presented in the study are included in the article/Supplementary Material, further inquiries can be directed to the corresponding authors.

## Author contributions

All authors discussed the results and commented on the manuscript, contributed to the article, and approved the submitted version.

## Funding

This work was supported by the Natural Science Basic Research Program of Shaanxi (Program no. 2020JQ-524).

## Acknowledgments

We would like to thank Editage ([www.editage.cn](http://www.editage.cn)) for English language editing.

## Conflict of interest

The authors declare that the research was conducted in the absence of any commercial or financial relationships that could be construed as a potential conflict of interest.

## Publisher's note

All claims expressed in this article are solely those of the authors and do not necessarily represent those of their affiliated organizations, or those of the publisher, the editors and the

reviewers. Any product that may be evaluated in this article, or claim that may be made by its manufacturer, is not guaranteed or endorsed by the publisher.

## Supplementary material

The Supplementary Material for this article can be found online at: <https://www.frontiersin.org/articles/10.3389/fmed.2022.799145/full#supplementary-material>

### SUPPLEMENTARY FIGURE 1

Red fluorescent signal of untreated SKOV-3 cells.

### SUPPLEMENTARY FIGURE 2

Red fluorescent signal of SKOV-3 cells with 10  $\mu\text{g/ml}$   $\text{Fe}_3\text{O}_4$  nanoparticles.

### SUPPLEMENTARY FIGURE 3

Red fluorescent signal of SKOV-3 cells with 10  $\mu\text{g/ml}$  CS- $\text{Fe}_3\text{O}_4$  nanoparticles.

### SUPPLEMENTARY METHOD: 2.5.4

EDU cell proliferation assay: The effect of  $\text{Fe}_3\text{O}_4$  and CS- $\text{Fe}_3\text{O}_4$  on SKOV-3 cell proliferation was also measured by EDU staining (BeyoClick EdU Cell Proliferation Kit with Alexa Fluor 488, Beyotime, China) incorporation assay as recommended by the manufacturer.

### SUPPLEMENTARY FIGURE 4

The cell viability effects of  $\text{Fe}_3\text{O}_4$  and CS- $\text{Fe}_3\text{O}_4$  nanoparticles with different pH value on SKOV-3 cells for 24 h through EDU staining.

## References

- Kornovski Y, Ivanova Y, Kostov S, Slavchev S, Yordanov A. Gynaecological oncologic diseases and pregnancy. *Wiad Lek.* (2021) 74:1984–7.
- Bentivegna E, Maulard A, Mialhe G, Gouy S, Morice P. Gynaecologic cancer surgery and preservation of fertility. *J Visc Surg.* (2018) 155:S23–9.
- Garcia J, Hurwitz HI, Sandler AB, Miles D, Coleman RL, Deurloo R, et al. Bevacizumab (Avastin®) in cancer treatment: a review of 15 years of clinical experience and future outlook. *Cancer Treat Rev.* (2020) 86:102017. doi: 10.1016/j.ctrv.2020.102017
- Bell SG, Uppal S, Sakala MD, Sciallis AP, Rolston A. An extrauterine extensively metastatic epithelioid trophoblastic tumor responsive to pembrolizumab. *Gynecol Oncol Rep.* (2021) 37:100819. doi: 10.1016/j.gore.2021.100819
- Monk BJ, Coleman RL, Fujiwara K, Wilson MK, Oza AM, Oaknin A, et al. ATHENA (GOG-3020/ENGOT-ov45): a randomized, phase III trial to evaluate rucaparib as monotherapy (ATHENA-MONO) and rucaparib in combination with nivolumab (ATHENA-COMBO) as maintenance treatment following frontline platinum-based chemotherapy in ovarian cancer. *Int J Gynecol Cancer.* (2021) 31:1589–94. doi: 10.1136/ijgc-2021-002933
- Paterniti TA, Dorr K, Ullah A, White J, Williams H, Ghamande S. Complete response to combination nivolumab and ipilimumab in recurrent neuroendocrine carcinoma of the cervix. *Obstet Gynecol.* (2021) 138:813–6. doi: 10.1097/AOG.0000000000004573
- Hamanishi J, Takeshima N, Katsumata N, Ushijima K, Kimura T, Takeuchi S, et al. Nivolumab versus gemcitabine or pegylated liposomal doxorubicin for patients with platinum-resistant ovarian cancer: open-label, randomized trial in Japan (NINJA). *J Clin Oncol.* (2021) 39:3671–81.
- Lazaratos M, Karathanou K, Mainas E, Chatzigoulas A, Pippa N, Demetzos C, et al. Coating of magnetic nanoparticles affects their interactions with model cell membranes. *Biochim Biophys Acta Gen Subj.* (2020) 1864:129671.
- Treuel L, Jiang X, Nienhaus GU. New views on cellular uptake and trafficking of manufactured nanoparticles. *J R Soc Interface.* (2013) 10:20120939. doi: 10.1098/rsif.2012.0939
- Hoshyar N, Gray S, Han H, Bao G. The effect of nanoparticle size on in vivo pharmacokinetics and cellular interaction. *Nanomedicine.* (2016) 11:673–92.
- Chowdhury HH, Cerqueira SR, Sousa N, Oliveira JM, Reis RL, Zorec R. The uptake, retention and clearance of drug-loaded dendrimer nanoparticles in astrocytes - electrophysiological quantification. *Biomater Sci.* (2018) 6:388–97. doi: 10.1039/c7bm00886d
- Vyas SP, Goswami R. Size-dependent cellular uptake and TLR4 attenuation by gold nanoparticles in lung adenocarcinoma cells. *Nanomedicine.* (2019) 14:229–53. doi: 10.2217/nnm-2018-0266
- Zhang S, Xu W, Gao P, Chen W, Zhou Q. Construction of dual nanomedicines for the imaging and alleviation of atherosclerosis. *Artif Cells Nanomed Biotechnol.* (2020) 48:169–79. doi: 10.1080/21691401.2019.1699823
- Zhang L, Xue H, Gao C, Carr L, Wang J, Chu B, et al. Imaging and cell targeting characteristics of magnetic nanoparticles modified by a functionalizable zwitterionic polymer with adhesive 3,4-dihydroxyphenyl-L-alanine linkages. *Biomaterials.* (2010) 31:6582–8. doi: 10.1016/j.biomaterials.2010.05.018
- Lee JH, Jang JT, Choi JS, Moon SH, Noh SH, Kim JW, et al. Exchange-coupled magnetic nanoparticles for efficient heat induction. *Nat Nanotechnol.* (2011) 6:418. doi: 10.1038/nnano.2011.95
- Morteza M, Sahraian MA, Shokrgozar MA, Sophie L. Superparamagnetic iron oxide nanoparticles: promises for diagnosis and treatment of multiple sclerosis. *Int J Mol Epidemiol Genet.* (2011) 2:367.
- Yang HW, Hua MY, Liu HL, Huang CY, Tsai RY, Lu YJ, et al. Self-protecting core-shell magnetic nanoparticles for targeted, traceable, long half-life delivery of BCNU to gliomas. *Biomaterials.* (2011) 32:6523–32. doi: 10.1016/j.biomaterials.2011.05.047
- Zou M, Xu P, Wang L, Wang L, Li T, Liu C, et al. Design and construction of a magnetic targeting pro-coagulant protein for embolic therapy of solid tumors. *Artif Cells Nanomed Biotechnol.* (2020) 48:116–28. doi: 10.1080/21691401.2019.1699817
- Patitsa M, Karathanou K, Kanaki Z, Tzioga L, Pippa N, Demetzos C, et al. Magnetic nanoparticles coated with polyarabic acid demonstrate enhanced drug

delivery and imaging properties for cancer theranostic applications. *Sci Rep.* (2017) 7:775. doi: 10.1038/s41598-017-00836-y

20. Chen Y, Bothun GD. Cationic gel-phase liposomes with "decorated" anionic spio nanoparticles: morphology, colloidal, and bilayer properties. *Langmuir.* (2011) 27:8645–52. doi: 10.1021/la2011138

21. Park SH, Oh SG, Mun JY, Han SS. Effects of silver nanoparticles on the fluidity of bilayer in phospholipid liposome. *Colloids And Surf B Biointerfaces.* (2005) 44:117–22. doi: 10.1016/j.colsurfb.2005.06.002

22. Revia RA, Zhang M. Magnetite nanoparticles for cancer diagnosis, treatment, and treatment monitoring: recent advances. *Mater Today.* (2016) 19:157–68.

23. Laurent S, Forge D, Port M, Roch A, Robic C, Elst LV, et al. Magnetic iron oxide nanoparticles: Synthesis, stabilization, vectorization, physicochemical characterizations, and biological applications. *Chem Rev.* (2008) 108:2064–110. doi: 10.1021/cr068445e

24. Rossi G, Monticelli L. Gold nanoparticles in model biological membranes: a computational perspective. *Biochim Biophys Acta.* (2016) 1858:2380–9. doi: 10.1016/j.bbamem.2016.04.001

25. Vacha R, Martinez-Veracochea FJ, Frenkel D. Receptor-mediated endocytosis of nanoparticles of various shapes. *Nano Lett.* (2011) 11:5391–5.

26. Chu M, Shao Y, Peng J, Dai X, Li H, Wu Q, et al. Near-infrared laser light mediated cancer therapy by photothermal effect of Fe<sub>3</sub>O<sub>4</sub> magnetic nanoparticles. *Biomaterials.* (2013) 34:4078–88.

27. Ao L, Wu C, Liu K, Wang W, Fang L, Huang L, et al. Polydopamine-derived hierarchical nanoplatforms for efficient dual-modal imaging-guided combination in vivo cancer therapy. *ACS Appl Mater Interfaces.* (2018) 10:12544–52. doi: 10.1021/acsami.8b02973

28. Wang X, Zhang J, Wang Y, Wang C, Xiao J, Zhang Q, et al. Multi-responsive photothermal-chemotherapy with drug-loaded melanin-like nanoparticles for synergetic tumor ablation. *Biomaterials.* (2016) 81:114–24. doi: 10.1016/j.biomaterials.2015.11.037

29. Liu Y, Guo Q, Zhu X, Feng W, Wang L, Ma L, et al. Optimization of prussian blue coated NaDyF<sub>4</sub>:x%Lu nanocomposites for multifunctional imaging-guided photothermal therapy. *Adv Funct Mater.* (2016) 26:5120–30.

30. Kievit FM, Zhang M. Surface engineering of iron oxide nanoparticles for targeted cancer therapy. *Acc Chem Res.* (2011) 44:853–62. doi: 10.1021/ar2000277

31. Heilmaier C, Lutz AM, Bolog N, Weishaupt D, Seifert B, Willmann JK. Focal liver lesions: detection and characterization at double-contrast liver MR imaging with ferucarbotran and gadobutrol versus single-contrast liver MR imaging. *Radiology.* (2009) 253:724–33. doi: 10.1148/radiol.2533090161

32. Kolosnjaj-Tabi J, Lartigue L, Javed Y, Luciani N, Pellegrino T, Wilhelm C, et al. Biotransformations of magnetic nanoparticles in the body. *Nano Today.* (2016) 11:280–4.

33. Seeney CE. The emerging applications of magnetic nanovectors in nanomedicine. *Pharm Patent Anal.* (2015) 4:285–304. doi: 10.4155/ppa.15.17

34. Fan X, Yuan Z, Shou C, Fan G, Wang H, Gao F, et al. cRGD-Conjugated Fe<sub>3</sub>O<sub>4</sub>@PDA-DOX multifunctional nanocomposites for MRI and antitumor chemo-photothermal therapy. *Int J Nanomed.* (2019) 14:9631–45. doi: 10.2147/IJN.S222797

35. Lu H, Wang W, Wang A. Ethanol–NaOH solidification method to intensify chitosan/poly(vinyl alcohol)/attapulgit composite film. *RSC Adv.* (2015) 5:17775–81.

36. Lu H, Ren S, Li X, Guo J, Dong G, Li J, et al. Poly(ethylene glycol)/chitosan/sodium glycerophosphate gel replaced the joint capsule with slow-release lubricant after joint surgery. *J Biomater Sci Polym Edn.* (2018) 29:1331–43. doi: 10.1080/09205063.2018.1459351

37. Lu H, Lv L, Ma J, Ban W, Ren S, Dong G, et al. Carbon dots intensified poly (ethylene glycol)/chitosan/sodium glycerophosphate hydrogel as artificial synovium tissue with slow-release lubricant. *J Mech Behav Biomed Mater.* (2018) 88:261–9. doi: 10.1016/j.jmbbm.2018.08.024

38. Lu H, Ren S, Guo J, Li Y, Li J, Dong G. Laser textured Co-Cr-Mo alloy stored chitosan/poly(ethylene glycol) composite applied on artificial joints lubrication. *Mater Sci Eng C Mater Biol Appl.* (2017) 78:239–45. doi: 10.1016/j.msec.2017.03.195

39. Javid A, Ahmadian S, Saboury AA, Kalantar SM, Rezaei-Zarchi S. Chitosan-coated superparamagnetic iron oxide nanoparticles for doxorubicin delivery: synthesis and anticancer effect against human ovarian cancer cells. *Chem Biol Drug Des.* (2013) 82:296–306. doi: 10.1111/cbdd.12145

40. Wen S. *Fourier Transform Infrared Spectrometry*. Pudong: Chemical Industry Press (2010).

41. Fathi M, Barar J, Erfan-Niya H, Omid Y. Methotrexate-conjugated chitosan-grafted pH- and thermo-responsive magnetic nanoparticles for targeted therapy of ovarian cancer. *Int J Biol Macromol.* (2020) 154:1175–84. doi: 10.1016/j.ijbiomac.2019.10.272